PCCP

PAPER

Cite this: *Phys. Chem. Chem. Phys.*, 2016, **18**, 25296

First-principles assessment of CO_2 capture mechanisms in aqueous piperazine solution†

Haley M. Stowe,[a] Eunsu Paek[b] and Gyeong S. Hwang*[ab]

Received 24th May 2016,
Accepted 15th August 2016

DOI: 10.1039/c6cp03584a

www.rsc.org/pccp

Piperazine (PZ) and its blends have emerged as attractive solvents for CO_2 capture, but the underlying reaction mechanisms still remain uncertain. Our study particularly focuses on assessing the relative roles of $PZCOO^-$ and PZH^+ produced from the PZ + CO_2 reaction. $PZCOO^-$ is found to directly react with CO_2 forming COO^-PZCOO^-, whereas PZH^+ will not. However, COO^-PZCOO^- appears very unlikely to be produced in thermodynamic equilibrium with monocarbamates, suggesting that its existence would predominantly originate from the surface reaction that likely occurs. We also find production of H^+PZCOO^- to be more probable with increasing CO_2 loading, due partly to the thermodynamic favorability of the $PZH^+ + PZCOO^- \rightarrow H^+PZCOO^- + PZ$ reaction; the facile PZ liberation may contribute to its relatively high CO_2 absorption rate. This study highlights an accurate description of surface reaction and the solvent composition effect is critical in thermodynamic and kinetic models for predicting the CO_2 capture processes.

1. Introduction

Energy-efficient and low-cost methods for capture of carbon dioxide (CO_2) from flue gases have been sought to curb greenhouse gas emissions while fossil fuels will likely remain a dominant energy source in the next few decades.[1,2] A wet-scrubbing approach using amines has been considered the most promising short-term solution.[3] Its widespread implementation is limited by the high cost associated with the high parasitic energy consumption during solvent regeneration, along with amine degradation and corrosion problems.[4–6] Various types of aqueous amines have been designed and tested for use in a post-combustion CO_2 capture plant.[7,8]

Aqueous piperazine (PZ) has been reported to have many advantageous qualities including low regeneration energy, low thermal and oxidative degradation rates, and low corrosivity relative to widely used alkanolamines such as monoethanolamine (MEA).[9–11] In addition, PZ exhibits a relatively high absorption rate and thus has been often used as a rate promoter in aqueous amine blends.[12–14] For instance, the rate of CO_2 absorption has been found to significantly increase when PZ is added to aqueous solutions of methyldiethanolamine (MDEA)[15–17] and 2-amino-2-methyl-1-propanol (AMP),[18,19] while reducing the regeneration energy. Although PZ has been typically used in small amounts (~5–10 wt%) due to solubility and viscosity concerns, recent studies have also proposed the use of concentrated PZ (~30–40 wt%) as the risk of solid precipitation tends to decrease under CO_2-loaded conditions.[9,10] While PZ-based amine solvents appear to be promising for post-combustion carbon capture, some fundamental aspects of CO_2 absorption in aqueous PZ solutions still remain unclear even though an accurate description of the reaction processes would be essential in efforts to optimize their performance.

Like various other amine solvents, CO_2 capture by aqueous PZ has been thought to occur *via* a two-step mechanism where PZ and CO_2 react to form a zwitterionic intermediate (PZ^+COO^-) followed by deprotonation to form carbamate ($PZCOO^-$);[20,21] the proton can be abstracted by available basic sites such as PZ forming protonated PZ (PZH^+).[22] Since each PZ has two basic N atoms, $PZCOO^-$ and PZH^+ may further participate in CO_2 capture. They may directly react with CO_2 to form dicarbamate (COO^-PZCOO^-) or protonated carbamate (H^+PZCOO^-). Likewise, the protonation/deprotonation processes can also be influenced by the presence of $PZCOO^-$ and PZH^+.

Several thermodynamic models have been proposed to predict the equilibrium concentrations of the PZ–CO_2 reaction products in aqueous solution as a function of CO_2 loading. The Gibbs free energy data have been largely extracted from nuclear magnetic resonance (NMR) measurements of the relative amounts of $PZ/PZH^+/H^+PZH^+$, $PZCOO^-/H^+PZCOO^-$, and COO^-PZCOO^-.[12,23] In NMR, however, the protonated and unprotonated forms of PZ and $PZCOO^-$ appear to be difficult to distinguish due to fast proton transfer. The relative concentrations of the

[a] *Materials Science and Engineering Program, University of Texas at Austin, Austin, Texas 78712, USA. E-mail: gshwang@che.utexas.edu; Fax: +1-512-471-7060; Tel: +1-512-471-4847*

[b] *McKetta Department of Chemical Engineering, University of Texas at Austin, Austin, Texas 78712, USA*

† Electronic supplementary information (ESI) available. See DOI: 10.1039/c6cp03584a

protonated/unprotonated species have been approximated using a thermodynamic equilibrium model with additional thermodynamic data such as pK_a values and CO_2 solubilities.[23–26] In addition, several kinetic studies have been undertaken to evaluate the CO_2 capture processes by PZ and its blends in aqueous solution.[12,14,22,27] In kinetic modeling, the elementary steps and their kinetics are mostly formulated based on experimental data; however, the detailed reaction mechanisms remain uncertain.

Static quantum mechanical (QM) calculations with various implicit solvation models have been employed to assess PZ's basicity and carbamate *versus* bicarbonate (HCO_3^-) formation with comparisons to other amine systems.[28–32] A similar approach has been used to evaluate the effect of different functional groups on the pK_a value of substituted PZ derivatives.[33] Very recently, formation of carbamate from a zwitterionic intermediate has been demonstrated by *ab initio* molecular dynamics (AIMD) simulations.[34] While these theoretical studies have been able to elucidate some properties of PZ, we still lack a full understanding of CO_2 absorption processes in PZ-based solutions, especially the relative roles played by PZH^+ and $PZCOO^-$.

In this work, we attempt to elucidate molecular mechanisms underlying the reaction of CO_2 with aqueous PZ using combined *ab initio* and classical force field calculations. First, we perform AIMD simulations to identify the elementary reactions involved in CO_2 capture by PZ in aqueous solution. Then, we assess the protonation behavior among PZ, $PZCOO^-$ and PZH^+ taking into account the solvation structure and dynamics using AIMD simulations combined with radial distribution function (RDF) analysis. In addition, we evaluate the interaction of CO_2 with $PZCOO^-$ and PZH^+, relative to PZ, by utilizing AIMD simulations to identify the reaction mechanisms involved and classical MD simulations for spatial distribution analysis of CO_2 around amine species. Thereafter, we estimate the relative thermodynamic favorabilities of reaction products in the H_2O–PZ–CO_2 system while accounting for solvent composition. The near-surface distributions of PZ and $PZCOO^-$, relative to other solvent species, are also analyzed to evaluate their relative contributions to CO_2 capture at the gas–solvent interface. The results of this study provide important insights into fundamental CO_2 absorption mechanisms in aqueous PZ solution. The improved mechanistic understanding may aid in the development of better kinetic and thermodynamic models to predict and optimize the performance of PZ in concentrated solution and as a rate-promoter in PZ-blends. Furthermore, it may provide valuable guidance on how to mitigate the disadvantages of PZ as well as in the design of new PZ-containing mixed solvents.

2. Computational methods

Ab initio molecular dynamics (AIMD) simulations based on density functional theory (DFT) were performed within the Born–Oppenheimer approximation using the Vienna ab initio Simulation Package (VASP).[35] The generalized gradient approximation (GGA) parametrized by Perdew, Burke and Ernzerhof (PBE)[36] was used for the exchange–correlation energy functional in restricted closed-shell DFT. We employed the projector augmented wave (PAW) method[37] to describe the interaction between core and valence electrons, and a planewave basis set with a kinetic energy cutoff of 400 eV; we verified that this energy cutoff is suitable in predicting the energetics for CO_2 capture by aqueous PZ (see the ESI†). Given the lack of symmetry and structure in aqueous solutions examined, we sampled the Brillouin zone using only one *k*-point (the gamma point).

The Gaussian 09 suite of programs[38] was used for the static quantum mechanical calculations at the B3LYP/6-311++G(d,p) level of theory. The SMD model of Truhlar and co-workers[39] within the polarizable continuum model (PCM) approach was used to estimate the solvation enthalpies and free energies of all species. The vibrational contributions to the free energy were estimated using the harmonic frequency analysis.

Classical MD simulations were performed using the Large-scale Atomic/Molecular Massively Parallel Simulator (LAMMPS) program.[40] We used the AMBER force field[41,42] for amine species ($PZ/PZH^+/PZCOO^-/H^+PZCOO^-/COO^-PZCOO^-$) with atomic charges obtained using the Merz–Singh–Kollman scheme.[43] These force field parameters are included in the ESI.† The SPC/E model[44] and a modified version of the EPM2 force field with flexible bonds and angles[45,46] were employed for H_2O and CO_2, respectively. All bonds involving H atoms were constrained using the SHAKE algorithm.[47] Spherical cutoffs of 10 Å and 12 Å were used for the Lennard-Jones and Coulomb interactions, respectively. Electrostatic interactions beyond the cutoff were calculated using the Ewald summation method.[48] Simulations were run in the *NVT* ensemble with a timestep of 1 fs. The temperature was controlled using a Nosé–Hoover thermostat[49] with a 100 fs damping parameter. Each simulated system was first annealed at 1000 K and then quenched to 323 K, followed by another annealing and quenching cycle. Production runs for the spatial distributions were carried out for 1 ns after the system is equilibrated.

The two-phase thermodynamics (2PT) method[50–52] was employed to calculate the absolute entropy of each aqueous amine system considered. This method has already been proven to be quite successful in predicting the entropy of a liquid system from a relatively short MD trajectory (10–20 ps) after equilibrium is reached.[50–53] In 2PT, the total entropy of a liquid system is given as a linear combination of gas-like and solid-like contributions, *i.e.*, $S_{tot} = f_g S_{gas} + (1 - f_g) S_{solid}$, where f_g (the fluidicity factor) is the gas-like fraction of the system; the gas-like component is modelled as a hard sphere gas and the solid-like portion is treated as a harmonic oscillator. It has been demonstrated that the f_g can be obtained in a self-consistent way from MD simulations.[50] For a liquid, the density of states (DOS) is decomposed into translational (S_{tra}), rotational (S_{rot}), and vibrational (S_{vib}), *i.e.*, $S(\nu) = S_{tra}(\nu) + S_{rot}(\nu) + S_{vib}(\nu)$. Here, the DOS is obtained from the Fourier transform of a velocity autocorrelation function. The translational and rotational contributions are calculated, respectively, from the center of mass and molecular angular velocities, while the vibrational component is determined from the remaining velocity after subtracting the translational and rotational contributions. For the 2PT analysis, velocities were

obtained from a trajectory of 30 ps in the *NVT* ensemble at 298 K for both AIMD and classical MD simulations where the trajectory files were recorded every 1 or 4 fs, respectively; the entropy values tend to converge after 20 ps, as shown in the ESI.† In order to enhance sampling of the small systems using AIMD simulations, we averaged the energies from at least 3 cases with different initial configurations.

3. Results and discussion

3.1. Proposed reaction mechanisms

Fig. 1 summarizes the probable routes during absorption of CO_2 into aqueous PZ solution that we propose based on our findings from this theoretical study, involving

- Reaction between PZ and CO_2 forming a zwitterionic intermediate [PZ + CO_2 → PZ^+COO^-] followed by deprotonation to produce PZ carbamate [PZ^+COO^- → $PZCOO^-$ + H^+]
- Reaction between $PZCOO^-$ and CO_2 to produce PZ dicarbamate following the two-step zwitterion mechanism [$PZCOO^-$ + CO_2 → $COO^-PZ^+COO^-$ → COO^-PZCOO^- + H^+]
- Protonation (deprotonation) of PZ (PZH^+) and $PZCOO^-$ (H^+PZCOO^-) [$PZ/PZCOO^-$ + H^+ ↔ PZH^+/H^+PZCOO^-]
- Direct reaction between PZH^+ and CO_2 as well as H^+PZH^+ formation are highly unlikely

In the following sections, we present the results of our investigations with emphasis on the relative tendencies of $PZ/PZCOO^-$/PZH^+ towards protonation and CO_2 reaction.

3.2. Demonstration of reaction of CO_2 with PZ in aqueous solution

We first performed AIMD simulations to examine the reaction of CO_2 with PZ in aqueous solution. AIMD has been proven to be a reliable option for identifying likely events and reaction intermediates in an aqueous amine–CO_2 system with a large number of degrees of freedom, while a static quantum chemical approach tends to be rather inadequate to account for the complex solution structure and dynamics.[54,55] We placed 2 PZ, 1 CO_2 and 20 H_2O molecules in a cubic simulation box of edge length 9.76 Å with periodic boundary conditions in all three directions, representing ≈30 wt% aqueous PZ; the corresponding density of 1.095 g cm^{-3} is well within experimental values at normal operating temperatures of 310–340 K.[56] The AIMD simulations were carried out at 400 K (*NVT* ensemble); this is below the thermal degradation temperature of 423 K.[10] The relatively high temperature was used in order to speed up the PZ–CO_2 reaction so as to identify probable elementary events within the limited simulation time span (~100 ps). This approach appears to be appropriate as rationalized in our previous papers.[54,55]

Fig. 2 displays the temporal variations in the total energy of the system as well as the distances between N (in PZ) and C (in CO_2) or H (originally attached to N in PZ) as indicated. Selected AIMD snapshots are also shown as insets. The total energy is found to gradually decrease as CO_2 approaches and reacts with PZ to form a zwitterionic adduct [(a) → (b), *i.e.*, PZ + CO_2 → PZ^+COO^-]. In the zwitterionic state, the N–C distance (d_{N-C}) varies between about 1.5 Å and 1.8 Å, and the noticeably increased N–H distance in PZ (d_{N-H}) fluctuates around 1.1 Å. Within 0.5 ps, the N-bound proton is transferred to the water network through a nearby H_2O molecule [(c) → (d), *i.e.*, PZ^+COO^- + H_2O → $PZCOO^-$ + H_3O^+], accompanied by a substantial energy drop. The deprotonation strengthens the N–C bond, as evidenced by the reduced d_{N-C} to 1.3 Å in the

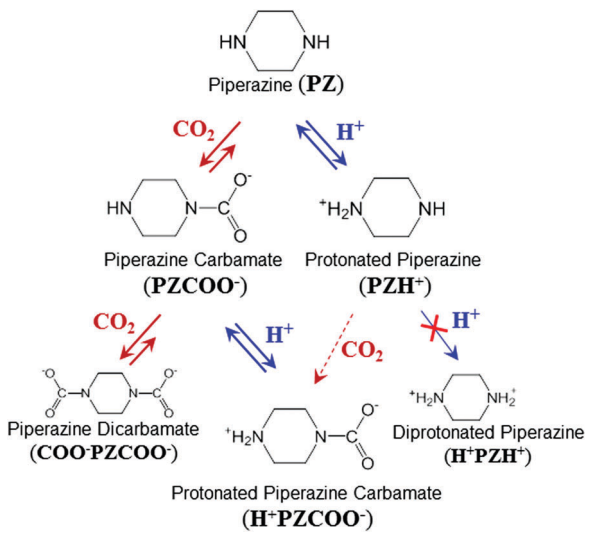

Fig. 1 Reaction routes for CO_2 absorption into aqueous piperazine (PZ) solution predicted or confirmed from this theoretical work. Protonated piperazine (PZH^+) may not directly react with CO_2 (indicated as a dashed line) and its protonation is unlikely (denoted by symbol X).

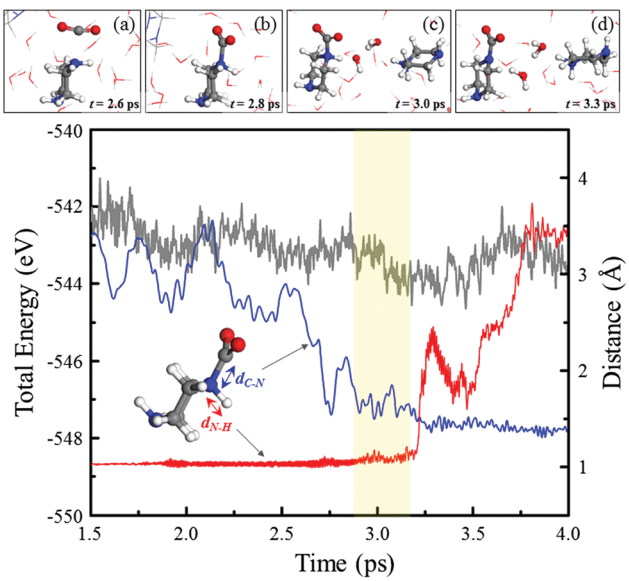

Fig. 2 Variations in the total energy (thick gray line) and the distances between C–N (blue line) and N–H (red line) in the zwitterionic intermediate during the 2PZ + CO_2 → PZH^+ + $PZCOO^-$ reaction from AIMD simulations at 400 K with the corresponding snapshots. The shaded region indicates when the zwitterionic intermediate is present. The system contains 2 PZ, 1 CO_2 and 20 H_2O molecules in a periodic cubic box with edge length 9.76 Å which represents approximately 30 wt% PZ. Red, gray, blue, and white balls represent O, C, N, and H atoms, respectively.

carbamate ($PZCOO^-$). The facile occurrence of deprotonation suggests that the activation barrier associated would be insignificant if neighboring H_2O molecules are arranged to allow for proton transfer to the water network. The solvated proton is subsequently abstracted by another PZ to form a protonated PZ [(c) → (d), *i.e.*, $H_3O^+ + PZ \rightarrow PZH^+$]. It would be also worthwhile to point out that, as shown in Fig. S1 in the ESI,† direct proton transfer from PZ^+COO^- to a nearby PZ was also observed in our AIMD simulations, although it is more likely that protons will be transferred through water bridges in aqueous solutions with 30 wt% concentration of PZ. In addition, our AIMD study demonstrates the possibility of proton abstraction by PZ from water due to its high basicity (*i.e.*, $PZ + H_2O \rightarrow OH^- + PZH^+$), but readily followed by protonation of OH^- in the presence of PZ^+COO^- and/or PZH^+ (*i.e.*, $OH^- + PZ^+COO^-/PZH^+ \rightarrow H_2O + PZCOO^-/PZ$).

The AIMD results clearly demonstrate that CO_2 is absorbed into aqueous PZ predominantly *via* the two-step zwitterion mechanism to produce $PZCOO^-$ and PZH^+ (*i.e.*, $2PZ + CO_2 \rightarrow PZ^+COO^- + PZ \rightarrow PZCOO^- + PZH^+$); this mechanism has been used to describe CO_2 absorption in other aqueous amines[20,21] as well as by amine-functionalized ionic liquids.[57,58] The preferred production of $PZCOO^-$ and PZH^+ at low CO_2 loading supports earlier experimental studies.[12,23] We also note that $PZCOO^-$ and PZH^+ may further participate in CO_2 absorption especially at higher CO_2 loadings, as each PZ has two basic N atoms. They may directly react with CO_2 to form PZ dicarbamate (COO^-PZCOO^-) or protonated PZ carbamate (H^+PZCOO^-), respectively. Likewise, the available N atoms in $PZCOO^-$ and PZH^+ may act as proton abstractors. The relative tendencies of PZ, $PZCOO^-$ and PZH^+ toward CO_2 capture and protonation can exert direct influence on the CO_2 capture process and the relative concentrations of products. Therefore, in the following sections, we will also examine how $PZCOO^-$ and PZH^+ interact with protons and CO_2, as compared to PZ.

3.3. Protonation behavior of PZ, PZH^+ and $PZCOO^-$

AIMD simulations were performed to examine the protonation tendencies of PZ, $PZCOO^-$ and PZH^+. Initially, 2 PZ, 1 H^+PZCOO^-, 1 PZH^+, and 45 H_2O molecules were placed in a cubic periodic box with edge length 12.37 Å, representing approximately 30 wt% PZ. We observed proton transfer between PZ and $PZCOO^-$ forming PZH^+ and H^+PZCOO^-, but not H^+PZH^+ formation. For example, Fig. 3 shows a series of AIMD snapshots during the proton transfer from H^+PZCOO^- to PZ. PZ abstracts a proton from H_2O [(a) → (b), *i.e.* $PZ + H_2O \rightarrow PZH^+ + OH^-$], while the proton in H^+PZCOO^- is released to OH^- [(b) → (c), *i.e.* $H^+PZCOO^- + OH^- \rightarrow PZCOO^- + H_2O$]; the process occurs rapidly, within 10 ps at 313 K.

We also explicitly considered the protonation behavior of PZ. Fig. 4 shows the temporal variation in the distance between each N in PZ (indicated as N_I or N_{II}) and H in its nearest H_2O neighbor (H_{H_2O}). Around 0.2 ps, N_I abstracts a proton from water to form PZH^+ (the N_I–H_{H_2O} distance fluctuates around 1.05 Å). Within the next 0.4 ps, the N_{II}–H_{H_2O} distance begins to decrease to about 1 Å as N_{II} is being protonated; simultaneously, the N_I–H_{H_2O} distance increases to above 1.5 Å, reflecting deprotonation. This clearly demonstrates that the N_I–H_{H_2O} and N_{II}–H_{H_2O} distances are inversely related to each other, reinforcing that H^+PZH^+ is unlikely to form although either of the N sites in PZ may be protonated.

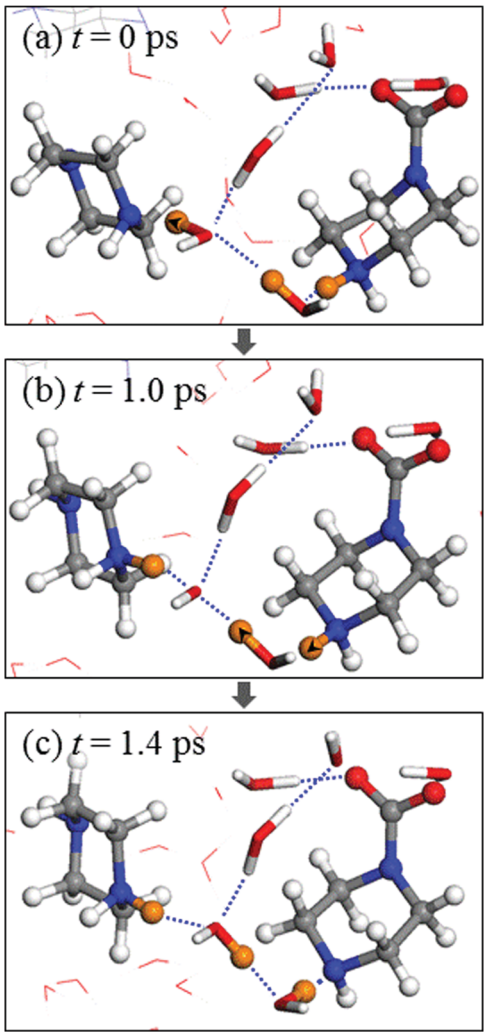

Fig. 3 AIMD snapshots demonstrating proton transfer through the hydrogen-bonded water network from H^+PZCOO^- to PZ at 313 K. Orange balls represent the atoms involved in this transfer reaction and blue dotted lines indicate hydrogen bonds.

The AIMD simulations imply that PZ and $PZCOO^-$ may act as proton abstractors whereas the protonation of PZH^+ may hardly take place, which can be expected by their relative basicities. The experimentally measured pK_a values for PZ and PZH^+ are 9.73 and 5.33,[59] respectively, and the pK_a value of $PZCOO^-$ has been estimated to be 9.15[12] and 9.44[22,23] based on NMR measurements of equilibrium constants.

In addition to the N sites, the O atoms in carbamate ($PZCOO^-$ or COO^-PZCOO^-) can also abstract a proton to form carbamic acid (PZCOOH or $COO^-PZCOOH$). However, the proton is easily released and tends to be more strongly bound to the N sites in PZ and $PZCOO^-$, according to our AIMD simulations. This is apparently because the O sites are less basic than the N sites; the predicted pK_a values for the former are 8.1–8.4, as compared to 9.5–9.8 for the latter obtained from our static QM calculations (further details are provided in the ESI†).

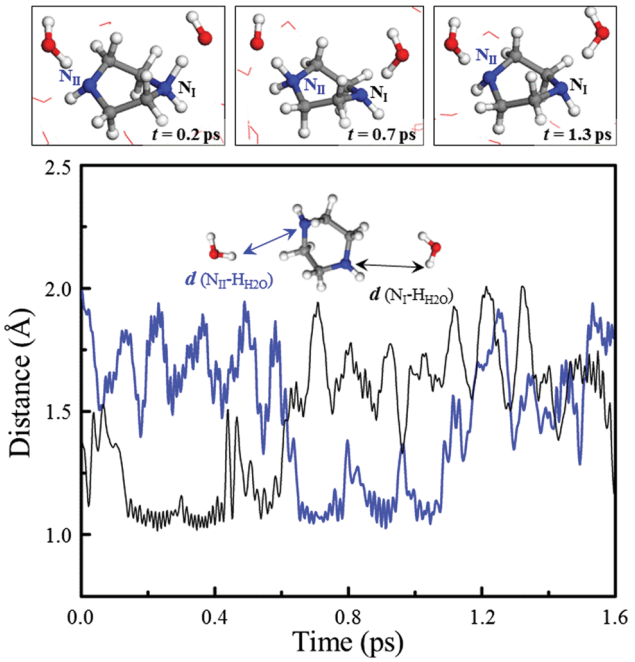

Fig. 4 Temporal variations in the distances between each N in PZ (indicated as N_I and N_{II}) and its nearest neighbor H in H_2O (H_{H_2O}) from AIMD simulations at 330 K. Black and blue lines indicate the N_I–H_{H_2O} and N_{II}–H_{H_2O} distances, respectively. Snapshots demonstrating protonation/deprotonation events with specified times in bold are also shown. The system consists of 1 PZ and 30 H_2O molecules in a cubic periodic box of edge length 10.11 Å.

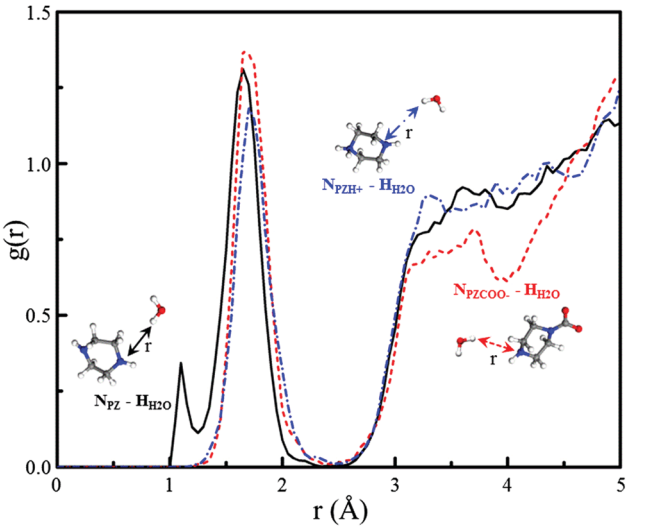

Fig. 5 Radial distribution functions between H in H_2O (H_{H_2O}) and basic N sites in PZ (N_{PZ}) (solid black line), $PZCOO^-$ (N_{PZCOO^-}) (dotted red line), and PZH^+ (N_{PZH^+}) (dashed-dotted blue line) predicted using AIMD simulations at 330 K. The systems consist of 30 H_2O and 1 PZ, 1 $PZCOO^-$ or 1 PZH^+ in a cubic periodic box of side length 10.11 Å, 10.34 Å, or 10.11 Å, respectively, corresponding to about 15 wt% PZ.

Next, we looked at the spatial arrangement of H_2O molecules around available N atoms in PZ (N_{PZ}), PZH^+ (N_{PZH^+}), and $PZCOO^-$ (N_{PZCOO^-}). Recall that proton transfer between amines in aqueous solution is largely mediated by water, implying that the protonation behavior would depend on not only the relative basicities of the N sites but also their connectivity through the hydrogen-bonded water network. As presented in Fig. 5, the radial distribution functions (RDFs, $g(r)$) were calculated to evaluate the respective pairwise interactions between $N_{PZ}/N_{PZH^+}/N_{PZCOO^-}$ and H in H_2O (H_{H_2O}) using AIMD simulations. The RDF is given by $g(r) = \langle n(r, r + dr)/4\pi r^2 \rho dr \rangle$, where $n(r, r + dr)$ is the number of atoms in a spherical shell of radius r (from the reference atom, N) with thickness dr and ρ is the bulk number density. Each system contains 30 H_2O and 1 PZ (PZH^+ or $PZCOO^-$) in a cubic periodic box with an edge length of 10.11 Å (10.11 Å or 10.34 Å), corresponding to about 15 wt% (the relatively dilute system was considered to minimize the direct interaction between amines). The AIMD simulations were run in the *NVE* ensemble for 5 ps, after being equilibrated in the *NVT* ensemble at 330 K for 5 ps. Each RDF plot was obtained from the average of at least 4 cases with different initial configurations.

The distinct peaks around 1.7 Å in Fig. 5 exhibit the attractive nature of the interaction between the positively charged H_{H_2O} and negatively charged N atoms. There is a noticeable shift in the peak positions, indicating that N_{PZ} interacts more strongly with neighboring H_2O compared to N_{PZCOO^-} and N_{PZH^+}. The integrated area under the peak (up to 2.5 Å where the minimum is located) shows the number of H_{H_2O} around the N atom. The predicted value of $\approx$1 in all three cases indicates that each N interacts with H_2O by forming a single hydrogen bond. In the aqueous solution of 10–30 wt% PZ, our analysis suggests that all possible base sites can be linked to each other *via* the hydrogen-bond network, which would allow rather fast proton transfer between them. Thus, the protonation tendencies of the N sites will be largely determined by their relative basicities and relative availabilities. Note also the small but distinct peak at 1.1 Å for the N_{PZ}–H_{H_2O} pair, which indicates abstraction of a proton from H_2O by PZ to form PZH^+ (*i.e.* PZ + H_2O → PZH^+ + OH^-). This peak is not visible in the cases of N_{PZCOO^-} and N_{PZH^+}, indicating their lower basicities relative to N_{PZ}.

Given the facile proton transfer between the N sites, the protonation/deprotonation processes can reach thermodynamic equilibrium under moderate temperature conditions. Therefore, the relative concentrations of $PZH^+/H^+PZCOO^-/H^+PZH^+$ could be estimated by the basicities and availabilities of $PZ/PZCOO^-/PZH^+$. Likewise, the concentrations of carbamate species ($PZCOO^-$, H^+PZCOO^-, COO^-PZCOO^-) have been evaluated based on their thermodynamic stabilities.[24,25] However, if CO_2 is not readily released from these PZ carbamates under typical absorber operating conditions, the carbamate concentrations may not be predicted only in terms of the thermodynamics aspect. In the following section, we will examine not only thermodynamic but also kinetic preference for CO_2 capture by PZH^+ and $PZCOO^-$, relative to PZ.

3.4. Comparison of interactions of CO_2 with PZ, PZH^+, and $PZCOO^-$

Reaction with CO_2. We first performed AIMD simulations at 400 K to examine the reaction of CO_2 with $PZCOO^-$ and PZH^+.

4 PZH^+, 4 $PZCOO^-$, 4 CO_2 and 8 H_2O molecules were placed in a periodic cubic box of edge length 12.066 Å. A relatively high concentration of CO_2/PZH^+/$PZCOO^-$ was used in order to speed up the possible amine–CO_2 reaction during the limited simulation time span by suppressing the hydration of the reactants; this should be a reasonable approach, as we attempt to demonstrate whether $PZCOO^-$ and PZH^+ may directly react with CO_2, rather than to evaluate their relative reaction rates. As seen in Fig. S2 in the ESI,† CO_2 is found to be captured by $PZCOO^-$ to form COO^-PZCOO^- *via* zwitterion formation and deprotonation. In the PZH^+ case, on the other hand, our AIMD simulations consistently show that PZH^+ is first deprotonated to become PZ, and then CO_2 reacts with PZ to form $PZCOO^-$ through a zwitterionic intermediate; the $PZCOO^-$ further abstracts a proton nearby to form H^+PZCOO^- (see Fig. 6). The AIMD results clearly demonstrate that PZ and $PZCOO^-$ can both react with CO_2 to form $PZCOO^-$ and COO^-PZCOO^-, respectively. On the other hand, PZH^+ is not likely to react directly with CO_2 to yield H^+PZCOO^-, which may not be surprising considering its low basicity; however, H^+PZCOO^- appears to easily form through protonation of $PZCOO^-$.

CO_2 accessibility. As we briefly mentioned above, the solvation shells around PZH^+ and $PZCOO^-$ may hinder the accessibility of CO_2 to the N_{PZH^+} and N_{PZCOO^-} sites. To further examine this effect, we performed classical MD simulations to evaluate the spatial distributions of CO_2 and H_2O around PZ, $PZCOO^-$, and PZH^+. Fig. 7 shows the pairwise RDFs between the centers of mass (COM) of PZ (PZH^+ or $PZCOO^-$) and H_2O [(a)], and between N_{PZ} (N_{PZH^+} or N_{PZCOO^-}) and C in CO_2 (C_{CO_2}) [(b)]. In addition, the corresponding spatial distribution functions (SDFs) between N_{PZ}/N_{PZH^+}/N_{PZCOO^-} and the COM of H_2O (O_{H_2O}) and CO_2 (C_{CO_2}) are presented in Fig. 7(c). The system contains 1605 H_2O, 49 PZ, 47 $PZCOO^-$, 47 PZH^+, and 16 CO_2 molecules in a cubical periodic box with an edge length of 41.34 Å. This represents approximately 30 wt% PZ at about 0.4 mol CO_2 per mol PZ loading; the density corresponds to 1.03 g cm^{-3}, which is in reasonable agreement with experiment.[56] Here, H^+PZCOO^- and COO^-PZCOO^- were not included because they are expected to have much lower concentrations than $PZCOO^-$/PZH^+ at this CO_2 loading level;[10,12,23] their presence is also not expected to significantly influence the interaction between PZ/PZH^+/$PZCOO^-$ and H_2O/CO_2 considering that the amount of water available relative to the amines is high at the concentration considered. The SDFs were calculated similarly to the RDFs, except that the atoms were not rotationally averaged around the reference atom, and therefore can be used to illustrate where the O_{H_2O} and C_{CO_2} atoms are most likely distributed around N_{PZ}/N_{PZH^+}/N_{PZCOO^-} in three-dimensional space; that is, the SDF is given by $g(\vec{r}) = \langle n(\vec{r}, \vec{r} + d\vec{r})/\rho d\vec{r} \rangle$, where $\vec{r}$ is the position of the surrounding atom in Cartesian coordinates from the reference atom N. For the SDF analysis, the simulation box must be rotated around each N so that the surrounding

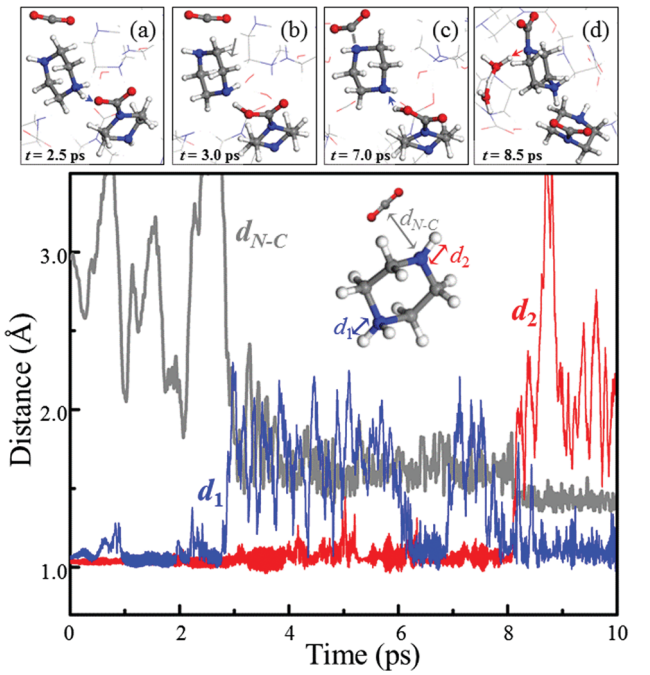

Fig. 6 Variations in the distances between N_{PZH^+} and C of CO_2 (d_{N-C}) (thick gray line), N_{PZH^+} and H/H^+ (d_2) (red line), and N and H^+ (d_1) (blue line) using AIMD simulations at 400 K. As also illustrated in the snapshots, first H^+ is released from PZH^+ at about 3 ps [(a) → (b)], indicated by increasing d_1. Then, d_{N-C} decreases as the PZ + CO_2 → PZ^+COO^- reaction occurs [(b) → (c)]. At about 8 ps [(d)], the zwitterionic intermediate is deprotonated followed by the protonation of $PZCOO^-$ forming H^+PZCOO^-; the former and latter are evidenced by the increase of d_2 and decrease of d_1, respectively. The system contains 4 $PZCOO^-$, 4 PZH^+ 4 CO_2 and 8 H_2O molecules in a cubic box with edge length 12.066 Å.

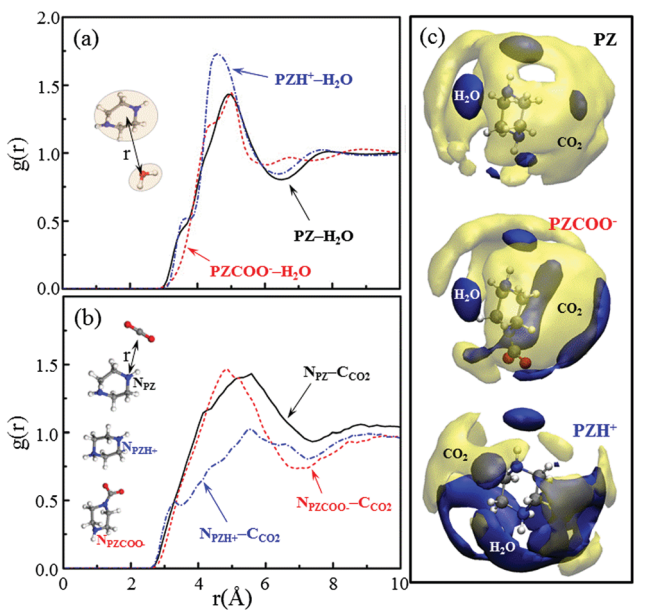

Fig. 7 Radial distribution functions for the pairs (a) between centers of mass of PZ, $PZCOO^-$ or PZH^+ and H_2O and (b) between N_{PZ}/N_{PZCOO^-}/N_{PZH^+} and C of CO_2 (C_{CO_2}), together with (c) spatial distribution functions with an isosurface threshold of 1.7 between N_{PZ}/N_{PZCOO^-}/N_{PZH^+} and O in H_2O (solid blue) or C in CO_2 (transparent yellow) using classical molecular dynamics simulations at 323 K. The system contains 1605 H_2O, 49 PZ, 47 $PZCOO^-$, 47 PZH^+, and 16 CO_2 molecules (representing 30 wt% PZ with 0.44 mol CO_2 per mol PZ) in a cubic simulation box of length 41.33 Å.

atoms are positioned from a reference orientation of amine; here, the plane containing N and the two adjacent C atoms in the PZ ring is chosen as the reference. The TRAVIS suite was utilized for the SDF analysis.[60] Both $g(r)$ and $g(\vec{r})$ were averaged from the snapshots generated every 500 fs over a trajectory of 1 ns.

As shown in Fig. 7(a), the first-peak intensity for the PZH^+–H_2O COM pair appears to be higher than the $PZCOO^-$ and PZ cases. The integrated areas under the first peak (up to 6.4 Å) are 24 for PZH^+ and 22 for $PZCOO^-$ and PZ, implying that H_2O molecules may more densely pack around PZH^+. It may be expected that H_2O would more densely pack around both PZH^+ and $PZCOO^-$ relative to PZ due to their excess positive/negative charge. The different solvation behavior is apparently attributed to the charge distribution in PZH^+/$PZCOO^-$. In the $PZCOO^-$ case, this excess charge is largely located on the CO_2 moiety (the charge of the carbamate portion is approximately -1.0 e^-), while the excess positive charge in PZH^+ is more evenly distributed around the ring, as shown in Table S12 (ESI†). Correspondingly, as illustrated in the SDFs [(c)], H_2O molecules are rather evenly distributed around PZH^+ whereas they tend to be localized around the –NH– group and the CO_2 moiety in the $PZCOO^-$ case. Also note that the partial atomic charges in the –NH– groups are similar among PZ, PZH^+, and $PZCOO^-$, leading to a similar distribution of H_2O near these groups in the SDFs; the N_{PZ}/N_{PZH^+}/N_{PZCOO^-} atoms have charges of about -0.7 e^-, and the corresponding H atoms attached to these N sites (H_N) have charges of about +0.35 e^- (see Table S12, ESI†).

Fig. 7(b) shows RDFs between N_{PZ}/N_{PZH^+}/N_{PZCOO^-} and C_{CO_2}. The first peaks for the N_{PZ}–C_{CO_2} and N_{PZCOO^-}–C_{CO_2} pairs are located at about 5 Å with similar intensity. For the N_{PZH^+}–C_{CO_2} pair, the first peak shifts to about 5.5 Å and has a relatively lower intensity. This demonstrates that CO_2 is less likely to approach N_{PZH^+} than N_{PZ} or N_{PZCOO^-}, implying that the even packing of H_2O around PZH^+ may impede CO_2 from approaching N_{PZH^+}. This suggests that the $PZH^+ + CO_2$ reaction may hardly occur, but H^+PZCOO^- can easily form through protonation of $PZCOO^-$. In the next section, we will discuss the relative thermodynamic favorability of $PZCOO^-$/H^+PZCOO^-/COO^-PZCOO^- production.

3.5. Thermodynamic prediction of $PZCOO^-$/H^+PZCOO^-/COO^-PZCOO^- formation

Reaction energetics for PZ + CO_2. The total energy change (ΔE) for the $2PZ + CO_2(g) \rightarrow PZCOO^- + PZH^+$ reaction was calculated using AIMD simulations at 298 K. Each PZ, $PZCOO^-$, and PZH^+ molecule was placed in a cubic periodic box with 30 H_2O molecules, as described in Section 3.3. From 3–6 samples for each system, the average ΔE is predicted to be about -13 kcal per mol CO_2. Note that our calculation assumes that the PZ species are fully dispersed and well hydrated in 15 wt% solution; however, in reality they may also interact with each other especially in high CO_2-loaded concentrated solution, which could cause some discrepancies between the predicted and experimentally measured energies. Nonetheless, the predicted value is in reasonable agreement with the experimentally reported ΔH of about -17 kcal per mol CO_2 at low CO_2 loadings (where PZH^+ and $PZCOO^-$ are predominantly formed) in 7–40 wt% aqueous PZ solution;[61,62] in the PZ–CO_2–H_2O system considered, $\Delta H \approx \Delta E$ as the PV work is negligible.

Comparison of $PZCOO^-$/H^+PZCOO^-/COO^-PZCOO^- production. We evaluated the relative thermodynamic favorability for PZH^+, $PZCOO^-$, H^+PZCOO^-, and COO^-PZCOO^- production considering two possible major competing reactions depending on CO_2 loading.

$$PZH^+ + PZCOO^- \leftrightarrow PZ + H^+PZCOO^- \quad (<0.5 \text{ mol } CO_2 \text{ per mol PZ}) \quad (A)$$

$$PZCOO^- + H^+PZCOO^- \leftrightarrow COO^-PZCOO^- + PZH^+ \quad (>0.5 \text{ mol } CO_2 \text{ per mol PZ}) \quad (B)$$

Helmholtz free energy changes ($\Delta A = \Delta E - T\Delta S$) for these reactions were estimated by calculating ΔE and ΔS using AIMD simulations at 298 K; free energy and enthalpy change predictions of the aforementioned reactions using static QM calculations are included in the ESI.† As described above, each PZ, $PZCOO^-$, PZH^+, H^+PZCOO^- and COO^-PZCOO^- molecule was placed in a cubic periodic box with 30 H_2O molecules corresponding to approximately 15 wt% solution where the molecules are assumed to be fully dispersed; box sizes are specified in the ESI.†

As listed in Table 1, ΔA is predicted to be about -2 kcal mol^{-1} for the $PZH^+ + PZCOO^- \rightarrow PZ + H^+PZCOO^-$ reaction; this indicates that protonation at the N_{PZ} site can be energetically comparable to the N_{PZCOO^-} site, particularly considering uncertainties in the predicted values ($\approx \pm$1–2 kcal mol^{-1}). A similar favorability is consistent with experimental observations that PZ has a similar pK_a value to $PZCOO^-$ in dilute aqueous solution;[12,22,23,59] ΔG estimated from experimentally reported pK_a values varies between 0.17 and 0.34 kcal mol^{-1}. The small ΔA (ΔG) is also in agreement with the facile proton transfer between N_{PZ} and N_{PZCOO^-} as observed from our AIMD simulations in Section 3.3. This suggests that the relative concentrations of protonated species (PZH^+/H^+PZCOO^-) would be dependent on the relative availability of PZ/$PZCOO^-$; at low CO_2 loadings, formation of PZH^+ and $PZCOO^-$ would be expected to be dominant due to the greater availability of PZ relative to $PZCOO^-$.

The $PZCOO^- + H^+PZCOO^- \rightarrow COO^-PZCOO^- + PZH^+$ reaction is predicted to be endergonic by $\Delta A \approx 4$ kcal mol^{-1} at room temperature. This implies that dicarbamate formation would be less probable with respect to monocarbamates. In addition, the positive ΔE ($\approx$3 kcal mol^{-1}) may indicate that the $PZCOO^-$/H^+PZCOO^- pair is more strongly solvated by water than the

Table 1 Predicted changes in the total energy (ΔE in kcal per mol CO_2), entropy (ΔS in cal per mol CO_2 per K), and Helmholtz free energy (ΔA in kcal per mol CO_2) obtained using AIMD simulations at 298 K for the listed reactions in aqueous solution. Each PZ, $PZCOO^-$, PZH^+, H^+PZCOO^- or COO^-PZCOO^- was placed in a cubic periodic box with 30 H_2O molecules, corresponding to approximately 15 wt%; further details of simulation conditions can be found in the ESI

Reaction	ΔE	ΔS	ΔA
$PZH^+ + PZCOO^- \rightarrow PZ + H^+PZCOO^-$	−7.9	−19.7	−2.0
$PZCOO^- + H^+PZCOO^- \rightarrow PZH^+ + COO^-PZCOO^-$	2.8	−3.6	3.9

COO^-PZCOO^-/PZH^+ pair. We also find that the ΔS is mostly due to the change in the translational entropy of water; the translational, rotational, and vibrational contributions of water and amine species for each system are summarized in Table S6 (ESI†). This suggests that the relative stability of the different carbamate products is largely determined by their interactions with water.

Recall that in the AIMD simulations, each system contains a single amine molecule, not accounting for possible amine–amine interactions. However, in concentrated solution amine species may undergo agglomeration, which would affect the solvation properties and in turn the thermodynamic favorabilities. According to our additional AIMD simulations where amine species are allowed to interact (see the ESI†), ΔS tends to be rather sensitive to amine agglomeration while ΔE is less significant to the variation of the solvent structure.

To further examine the possible effect of amine agglomeration on ΔS, we performed classical MD simulations by varying the PZ concentration and CO_2 loading at 298 K. As summarized in Table 2, the following three cases were considered for reaction (A): (i) 15 wt% PZ at 0.16 CO_2 loading, (ii) 30 wt% PZ at 0.16 CO_2 loading, and (iii) 30 wt% PZ at 0.33 CO_2 loading. Accounting for the change in configurational entropy does not alter the relative entropic favorabilities as presented in Tables 2 and 3 (see the ESI†).

In cases (i), (ii), and (iii), ΔS is predicted to be 13–14 cal per mol CO_2 per K, demonstrating that the $PZH^+ + PZCOO^- \rightarrow PZ + H^+PZCOO^-$ reaction is entropically favorable. The unfavorable entropic change for this reaction from the AIMD simulations is likely because the amines are well-dispersed, whereas in the classical MD simulations the amines may aggregate; similar entropy changes to those shown in Table 1 were predicted using classical MD simulations when the amines are well-dispersed (see the ESI†). Note that while ΔS of the amines does not vary widely among the three cases, there is a slight increase in ΔS of water (from 1.05 to 2.21 and 4.76 cal per mol CO_2 per K in cases (i) to (ii) and (iii)). This is likely related to agglomeration of PZH^+ and $PZCOO^-$ which occurs more strongly as their concentrations increase. With increasing amine agglomeration, the hydrogen-bonded water network is less perturbed due to the reduced amine–water interaction, thereby decreasing the entropy of water; the larger reduction in the entropy of water for systems with more $PZH^+/PZCOO^-$ pairs is further shown in the ESI.† This analysis suggests that the formation of H^+PZCOO^- relative to PZH^+ would be dependent on the availability of $PZCOO^-$ relative to PZ. At high CO_2 loadings, PZ liberation may also be facile due to the thermodynamic favorability of formation of H^+PZCOO^- from $PZH^+/PZCOO^-$; this could contribute to the high CO_2 absorption rate of PZ as observed experimentally.[12–14]

In the case of reaction (B), we also estimated how ΔS changes with the relative formation of monocarbamate and dicarbamate. Here, only 30 wt% PZ at 0.67 CO_2 loading was considered. As summarized in Table 3, in case (iv), ΔS is predicted to be −2.8 cal per mol CO_2 per K as 20% of $H^+PZCOO^-/PZCOO^-$ converts to COO^-PZCOO^-/PZH^+. Upon increasing the conversion to 50% [case (v)] and 100% [case (vi)], ΔS becomes more negative at −6.8, and −9.9 cal per mol CO_2 per K, respectively. This clearly indicates that dicarbamate formation is entropically unfavorable relative to monocarbamates, which is largely due to the entropy of water (ΔS_{H_2O} = −2.5, −5.2, and −6.9 cal per mol CO_2 per K in cases (iv), (v), and (vi), respectively). Given sizable negative ΔS and positive ΔE leading to highly positive ΔA ($=\Delta E - T\Delta S$), the $PZCOO^- + H^+PZCOO^- \rightarrow COO^-PZCOO^- + PZH^+$ reaction may be thermodynamically unlikely.

Our thermodynamic analysis suggests that at low CO_2 loadings, PZH^+ and $PZCOO^-$ will predominantly form. With increasing CO_2 loading, H^+PZCOO^- production will gradually increase as (i) free PZ becomes less available for proton abstraction and (ii) the $PZH^+ + PZCOO^- \rightarrow PZ + H^+PZCOO^-$ reaction is thermodynamically favorable. This prediction is consistent with equilibrium speciation data generated by NMR measurements and thermodynamic equilibrium models which find PZH^+ and $PZCOO^-$ to predominantly form at low loadings, while H^+PZCOO^- predominantly forms at high CO_2 loadings.[12,23] However, according to our free energy estimations, COO^-PZCOO^- formation is highly unlikely relative to $PZCOO^-/H^+PZCOO^-$ in thermodynamic equilibrium, which is in contrast to experimental studies reporting the presence of dicarbamates at high CO_2 loadings, albeit in a relatively small amount.[12,23]

3.6. Role of surface reactions in dicarbamate production

Although COO^-PZCOO^- formation may not be thermodynamically favorable in highly CO_2-loaded concentrated PZ solutions, our AIMD simulations and RDF analysis (see Section 3.4) suggest that CO_2 capture by $PZCOO^-$ to form COO^-PZCOO^- is not kinetically prohibited. If COO^-PZCOO^- would form at the gas–solvent interface and does not easily release CO_2, it may not fully convert to thermodynamically preferred $PZCOO^-/H^+PZCOO^-$ in bulk solution during absorption operations. To examine the

Table 2 Predicted entropy changes ($\Delta S = S_P - S_R$ in cal per mol CO_2 per K) obtained using classical MD simulations at 298 K for the $PZH^+ + PZCOO^- \rightarrow PZ + H^+PZCOO^-$ reaction at varying PZ concentrations (wt%) and CO_2 loadings (α = mol CO_2 per mol PZ), as indicated. The decoupled contributions of H_2O and amines are also presented. The corresponding numbers of amine species in the reactant (S_R) and product (S_P) sides placed in a cubic periodic box with edge length (as specified in parenthesis) are also listed. Systems representing 15 (30) wt% PZ solution contain 1960 (1600) H_2O molecules

		Composition	
	ΔS ($=\Delta S_{H_2O} + \Delta S_{amine}$)	S_R (edge length)	S_P (edge length)
Case (i) (15 wt%, α = 0.16)	13.98 (=1.05 + 12.92)	51 PZ, 12 PZH^+, 12 $PZCOO^-$ (41.14 Å)	63 PZ, 12 H^+PZCOO^- (41.21 Å)
Case (ii) (30 wt%, α = 0.16)	13.25 (=2.21 + 11.04)	100 PZ, 25 PZH^+, 25 $PZCOO^-$ (41.07 Å)	125 PZ, 25 H^+PZCOO^- (41.17 Å)
Case (iii) (30 wt%, α = 0.33)	13.98 (=4.76 + 9.22)	50 PZ, 50 PZH^+, 50 $PZCOO^-$ (41.05 Å)	100 PZ, 50 H^+PZCOO^- (41.25 Å)

Table 3 Predicted entropy changes ($\Delta S = S_P - S_R$ in cal per mol CO_2 per K) obtained using classical MD simulations at 298 K for the $PZCOO^-$ + H^+PZCOO^- → COO^-PZCOO^- + PZH^+ reaction at varying conversions (X). The decoupled contributions of H_2O and amines are also presented. The corresponding numbers of amine species in the reactant (S_R) and product (S_P) sides placed in a cubic periodic box with edge length (as specified in parenthesis) are also listed. All systems represent 30 wt% PZ solution at 0.67 CO_2 loading and contain 1600 H_2O molecules

		Composition	
	ΔS (=ΔS_{H_2O} + ΔS_{amine})	S_R (edge length)	S_P (edge length)
Case (iv) (X = 20%)	−2.84 (=−2.51 + −0.32)	50 PZH^+, 50 $PZCOO^-$, 50 H^+PZCOO^- (41.25)	60 PZH^+, 40 $PZCOO^-$, 40 H^+PZCOO^-, 10 COO^-PZCOO^- (41.17)
Case (v) (X = 50%)	−6.84 (=−5.18 + −1.66)		75 PZH^+, 25 $PZCOO^-$, 25 H^+PZCOO^-, 25 COO^-PZCOO^- (41.08)
Case (vi) (X = 100%)	−9.92 (=−6.95 + −2.97)		100 PZH^+, 50 COO^-PZCOO^- (40.92)

possibility for CO_2 reaction with $PZCOO^-$, we calculated the near-surface distributions of amine species in CO_2-loaded aqueous PZ solution using classical MD simulations at 323 K. The surface was modeled using a slab system consisting of 8777 H_2O, 200 PZ, 169 $PZCOO^-$, 269 PZH^+, 100 H^+PZCOO^- and 50 COO^-PZCOO^- molecules (representing 30 wt% PZ at about 0.5 CO_2 loading) in a 50 Å × 50 Å × 150 Å box.

Fig. 8(a) shows atomic distributions for N_{PZ}, N_{PZCOO^-}, and N_{PZH^+} near the solvent surface, along with COM distributions of H_2O, PZ, $PZCOO^-$, PZH^+, H^+PZCOO^-, and COO^-PZCOO^- in (b). In Fig. 8(a), the C of CO_2 (C_{CO_2}) adsorbed in the PZ solution is also presented to demonstrate its relative contact with amines. This analysis clearly shows that PZ tends to accumulate at the gas–solvent interface, as also seen with other amines in aqueous solution.[63] Some $PZCOO^-$ and PZH^+ are also present near the surface, while H^+PZCOO^- and COO^-PZCOO^- exist farther into the bulk. Looking at the relative distributions of the N sites (N_{PZ}, N_{PZCOO^-}, and N_{PZH^+}) possibly available for CO_2 capture, N_{PZ} is located closest to the surface where C_{CO_2} accumulates mostly, followed by N_{PZCOO^-} and N_{PZH^+}. The strong tendency of surface accumulation of PZ may be another factor for its exceptionally high absorption rate relative to other aqueous amines. Although surface accumulation has also been observed for other amines such as MEA,[63] this effect is expected to be enhanced in the case of PZ due to its much lower solubility relative to other commonly used amines for CO_2 capture.[64] Notice also an overlap between N_{PZCOO^-} and C_{CO_2} near the surface, which may suggest possible occurrence of the reaction between $PZCOO^-$ and CO_2 forming COO^-PZCOO^-. The likelihood of the $PZCOO^-$ + CO_2 → COO^-PZCOO^- reaction may increase as free PZ depletes with the progression of CO_2 absorption. Although we do not attempt to estimate reaction rates herein, our analysis suggests that CO_2 predominantly reacts with PZ, while the $PZCOO^-$–CO_2 reaction occurs to a lesser extent at high CO_2 loadings; the PZH^+–CO_2 reaction hardly occurs. This is in qualitative agreement with kinetic studies evaluating the relative reaction rates of $PZ/PZCOO^-/PZH^+$ with CO_2.[14,22]

This analysis reiterates that dicarbamate (COO^-PZCOO^-) production likely originates from CO_2 capture by $PZCOO^-$ near the surface, rather than its interconversion with monocarbamates ($PZCOO^-/H^+PZCOO^-$) at thermodynamic equilibrium in the bulk. Perhaps, NMR spectroscopy combined with isotope labelling could be used to prove whether or not interconversion between monocarbamate and dicarbamate easily occurs under typical absorber operating conditions. Nonetheless, this study highlights the importance of considering the near-surface composition and its possible influence on modeling/predicting the performance of aqueous amine systems, especially when more than one amine species are involved in CO_2 capture.

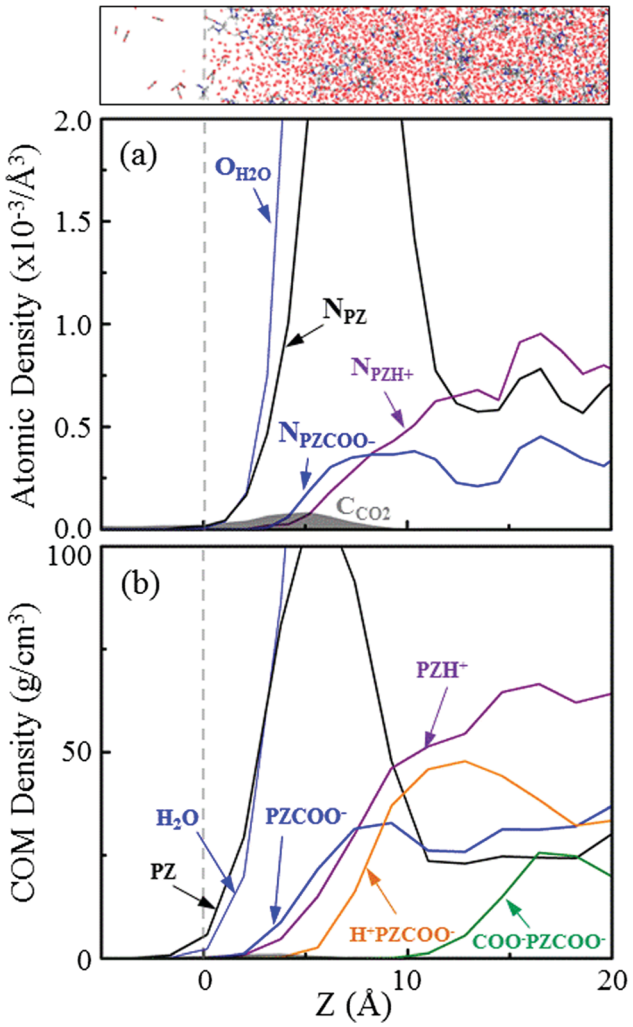

Fig. 8 (a) Near-surface distributions of N_{PZ}, N_{PZCOO^-}, and N_{PZH^+} and (b) COM distributions of H_2O, PZ, $PZCOO^-$, PZH^+, H^+PZCOO^-, and COO^-PZCOO^- using classical MD simulations at 323 K with a slab system representing 30 wt% PZ at about 0.5 CO_2 loading. The distribution of C_{CO_2} (shaded gray) included in (a) has been adjusted to represent P_{CO_2} = 1 bar.

3.7. Summary of studies and findings

In this section, we summarize our findings regarding the underlying mechanisms of CO_2 capture by aqueous PZ using combined DFT and force field calculations.

• DFT-based AIMD simulations clearly show that PZ reacts with CO_2 to form $PZCOO^-$ and PZH^+ *via* the two-step zwitterion mechanism, *i.e.*, $2PZ + CO_2 \rightarrow PZ^+COO^- + PZ \rightarrow PZCOO^- + PZH^+$, which is consistent with previous experimental studies reporting the preferred production of $PZCOO^-$ and PZH^+ at low CO_2 loadings.

• Our AIMD simulations combined with RDF analysis confirms that PZ and $PZCOO^-$ may act as proton abstractors, whereas the protonation of PZH^+ hardly takes place. We also observed proton transfer between the N and O of amines to occur rather rapidly while the available basic sites are well-linked *via* the hydrogen bond network in CO_2-loaded aqueous PZ solution. As such, the relative concentrations of protonated amine species can be determined by their thermodynamic favorability for protonation under typical absorber operating conditions.

• While PZ and $PZCOO^-$ compete for proton abstraction, *i.e.*, $PZH^+ + PZCOO^- \leftrightarrow PZ + H^+PZCOO^-$, the production of H^+PZCOO^- is found to be more probable with increasing CO_2 loading. This is not only because less PZ is available relative to $PZCOO^-$ but also because proton transfer from PZH^+ to $PZCOO^-$ (forming H^+PZCOO^- and liberating PZ) is thermodynamically favorable. According to our free energy calculations, $PZH^+/PZCOO^-$ is less entropically favorable in comparison to PZ/H^+PZCOO^-; we attribute this largely to their stronger tendency to aggregate, leading to a greater reduction in the entropy of water as the hydrogen bond network is less perturbed. This also highlights the important role played by solvent restructuring associated with amine aggregation in determining the relative stability of amine–CO_2 reaction products.

• Regarding CO_2 reaction with PZH^+ and $PZCOO^-$, we find that $PZCOO^-$ can readily react with CO_2 to form COO^-PZCOO^-, however the reaction between PZH^+ and CO_2 may hardly occur. Our AIMD simulations consistently show that PZH^+ first releases the proton and then free PZ undergoes reaction with CO_2 to form $PZCOO^-$ (which can subsequently abstract a proton to form H^+PZCOO^-). This is largely attributed to the low basicity of PZH^+. Moreover, according to spatial distribution analysis using classical MD simulations, water molecules tend to be more densely packed around PZH^+, relative to PZ and $PZCOO^-$, which may hinder CO_2 accessibility and thus further suppress the $PZH^+ + CO_2$ reaction.

• Although CO_2 capture by $PZCOO^-$ may not be kinetically prohibited, our free energy calculations predict COO^-PZCOO^- production to be far less thermodynamically favorable relative to monocarbamates ($PZCOO^-/H^+PZCOO^-$). This suggests that the existence of COO^-PZCOO^- tends to be highly unlikely in thermodynamic equilibrium. However, previous experimental studies report the presence of COO^-PZCOO^- at high CO_2 loadings, albeit in a relatively small amount.

• Analysis of the near-surface distributions of PZ, $PZCOO^-$, and other amines shows that the available N in $PZCOO^-$ (N_{PZCOO^-}) remains near the gas–solvent interface although PZ is located closest to the surface where CO_2 accumulates. This suggests that while CO_2 may be predominantly captured by PZ, the $PZCOO^- + CO_2 \rightarrow COO^-PZCOO^-$ reaction may possibly occur especially when PZ is depleted with increasing CO_2 loading. Based on our findings, we speculate that dicarbamate production originates from CO_2 capture by $PZCOO^-$ near the surface, rather than interconversion with monocarbamates in the bulk. Perhaps, NMR spectroscopy combined with isotope labelling could be used to prove whether or not the interconversion between COO^-PZCOO^- and $PZCOO^-/H^+PZCOO^-$ will reach thermodynamic equilibrium under typical absorber operating conditions.

4. Conclusions

We used combined DFT and force field calculations to examine the molecular mechanisms underlying CO_2 absorption into aqueous PZ, including the role of $PZCOO^-$ and PZH^+. Our studies and main findings are summarized in Section 3.7. A deeper understanding of the molecular mechanisms of reaction of CO_2 with PZ in aqueous solution may assist in efforts to develop better kinetic and thermodynamic models by improving the accuracy of the description of these reaction processes. Furthermore, the improved fundamental understanding may provide valuable guidance in the design of new PZ-containing mixed amine solvents.

Additionally, in conjunction with previous experimental and modeling studies, the results obtained in this work also lead us to speculate that:

• The exceptionally high CO_2 absorption rate of PZ relative to other amines may be attributed to (i) its strong tendency of surface accumulation and (ii) PZ liberation as a result of the thermodynamic favorability for the $PZH^+ + PZCOO^- \rightarrow PZ + H^+PZCOO^-$ reaction; the liberated PZ may then diffuse to the surface and contribute to CO_2 capture.

• CO_2 absorption into aqueous PZ likely occurs through the reaction with not only PZ but also $PZCOO^-$, and thus the absorption rate can be a function of their relative availability. Therefore, an accurate description of the near-surface distributions of PZ and $PZCOO^-$ would be critical in kinetic models for predicting CO_2 capture processes.

Acknowledgements

This work was supported by the Korea CCS R&D Center (KCRC) grant (no. 2015053544) funded by the Korea government (Ministry of Science, ICT & Future Planning) and the R. A. Welch Foundation (no. F-1535). We would like to thank the Texas Advanced Computing Center for use of the Stampede supercomputing system (OCI-1134872). Helpful discussions with Gary Rochelle and Hoon Sik Kim and assistance with calculations from Linas Vilčiauskas are also greatly acknowledged.

References

1 S. D. Kenarsari, D. Yang, G. Jiang, S. Zhang, J. Wang, A. G. Russell, Q. Wei and M. Fan, *RSC Adv.*, 2013, **3**, 22739–22773.

2 J. D. Figueroa, T. Fout, S. Plasynski, H. McIlvried and R. D. Srivastava, *Int. J. Greenhouse Gas Control*, 2008, **2**, 9–20.
3 G. T. Rochelle, *Science*, 2009, **325**, 1652–1654.
4 D. M. D'Alessandro, B. Smit and J. R. Long, *Angew. Chem., Int. Ed.*, 2010, **49**, 6058–6082.
5 B. R. Strazisar, R. R. Anderson and C. M. White, *Energy Fuels*, 2003, **17**, 1034–1039.
6 M. R. M. Abu-Zahra, L. H. J. Schneiders, J. P. M. Niederer, P. H. M. Feron and G. F. Versteeg, *Int. J. Greenhouse Gas Control*, 2007, **1**, 37–46.
7 M. Wang, A. Lawal, P. Stephenson, J. Sidders and C. Ramshaw, *Chem. Eng. Res. Des.*, 2011, **89**, 1609–1624.
8 G. Puxty, R. Rowland, A. Allport, Q. Yang, M. Bown, R. Burns, M. Maeder and M. Attalla, *Environ. Sci. Technol.*, 2009, **43**, 6427–6433.
9 S. A. Freeman, R. Dugas, D. H. Van Wagener, T. Nguyen and G. T. Rochelle, *Int. J. Greenhouse Gas Control*, 2010, **4**, 119–124.
10 G. Rochelle, E. Chen, S. Freeman, D. Van Wagener, Q. Xu and A. Voice, *Chem. Eng. J.*, 2011, **171**, 725–733.
11 L. Zheng, J. Landon, N. Matin, Z. Li, G. Qi and K. Liu, *ECS Trans.*, 2014, **61**, 81–95.
12 S. Bishnoi and G. T. Rochelle, *Chem. Eng. Sci.*, 2000, **55**, 5531–5543.
13 A. Samanta and S. S. Bandyopadhyay, *Chem. Eng. Sci.*, 2007, **62**, 7312–7319.
14 W. Conway, D. Fernandes, Y. Beyad, R. Burns, G. Lawrance, G. Puxty and M. Maeder, *J. Phys. Chem. A*, 2013, **117**, 806–813.
15 M. Appl, U. Wagner, H. J. Henrici, K. Kuessner, K. Volkamer and E. Fuerst, *Removal of CO_2 and/or H_2S and/or CO_2 from gases containing these constituents, US Pat., 4336233, 1982.*
16 G.-W. Xu, C.-F. Zhang, S.-J. Qin and Y.-W. Wang, *Ind. Eng. Chem. Res.*, 1992, **31**, 921–927.
17 S. Bishnoi and G. T. Rochelle, *AIChE J.*, 2002, **48**, 2788–2799.
18 D. J. Seo and W. H. Hong, *Ind. Eng. Chem. Res.*, 2000, **39**, 2062–2067.
19 W.-C. Sun, C.-B. Yong and M.-H. Li, *Chem. Eng. Sci.*, 2005, **60**, 503–516.
20 M. Caplow, *J. Am. Chem. Soc.*, 1968, **90**, 6795–6803.
21 P. V. Danckwerts, *Chem. Eng. Sci.*, 1979, **34**, 443–446.
22 P. W. J. Derks, T. Kleingeld, C. van Aken, J. A. Hogendoorn and G. F. Versteeg, *Chem. Eng. Sci.*, 2006, **61**, 6837–6854.
23 V. Ermatchkov, Á. Pérez-Salado Kamps and G. Maurer, *J. Chem. Thermodyn.*, 2003, **35**, 1277–1289.
24 Á. Pérez-Salado Kamps, J. Xia and G. Maurer, *AIChE J.*, 2003, **49**, 2662–2670.
25 P. W. J. Derks, H. B. S. Dijkstra, J. A. Hogendoorn and G. F. Versteeg, *AIChE J.*, 2005, **51**, 2311–2327.
26 S. K. Dash, A. Samanta, A. N. Samanta and S. S. Bandyopadhyay, *Fluid Phase Equilib.*, 2011, **300**, 145–154.
27 X. Zhang, C.-F. Zhang, S.-J. Qin and Z.-S. Zheng, *Ind. Eng. Chem. Res.*, 2001, **40**, 3785–3791.
28 E. F. da Silva, *J. Phys. Chem. A*, 2005, **109**, 1603–1607.
29 E. F. da Silva and H. F. Svendsen, *Ind. Eng. Chem. Res.*, 2006, **45**, 2497–2504.
30 E. F. da Silva and H. F. Svendsen, *Int. J. Greenhouse Gas Control*, 2007, **1**, 151–157.
31 P. Jackson, A. Beste and M. Attalla, *Struct. Chem.*, 2011, **22**, 537–549.
32 F. Khalili, A. Henni and A. L. L. East, *THEOCHEM*, 2009, **916**, 1–9.
33 S. Gangarapu, G. J. Wierda, A. T. M. Marcelis and H. Zuilhof, *ChemPhysChem*, 2014, **15**, 1880–1886.
34 K. Z. Sumon, A. Henni and A. L. L. East, *J. Phys. Chem. Lett.*, 2014, **5**, 1151–1156.
35 G. Kresse and J. Furthmuller, *Phys. Rev. B: Condens. Matter Mater. Phys.*, 1996, **54**, 11169–11186.
36 J. P. Perdew, K. Burke and M. Ernzerhof, *Phys. Rev. Lett.*, 1996, **77**, 3865–3868.
37 G. Kresse and D. Joubert, *Phys. Rev. B: Condens. Matter Mater. Phys.*, 1999, **59**, 1758–1775.
38 M. J. Frisch, G. W. Trucks, H. B. Schlegel, G. E. Scuseria, M. A. Robb, J. R. Cheeseman, G. Scalmani, V. Barone, B. Mennucci, G. A. Petersson, H. Nakatsuji, M. Caricato, X. Li, H. P. Hratchian, A. F. Izmaylov, J. Bloino, G. Zheng, J. L. Sonnenberg, M. Hada, M. Ehara, K. Toyota, R. Fukuda, J. Hasegawa, M. Ishida, T. Nakajima, Y. Honda, O. Kitao, H. Nakai, T. Vreven, J. A. Montgomery, J. E. Peralta, F. Ogliaro, M. Bearpark, J. J. Heyd, E. Brothers, K. N. Kudin, V. N. Staroverov, T. Keith, R. Kobayashi, J. Normald, K. Raghavachari, A. Rendell, J. C. Burant, S. S. Iyengar, J. Tomasi, M. Cossi, N. Rega, J. M. Millam, M. Klene, J. E. Knox, J. B. Cross, V. Bakken, C. Adamo, J. Jaramillo, R. Gomperts, R. E. Stratmann, O. Yazyev, A. J. Austin, R. Cammi, C. Pomelli, J. W. Ochterski, R. L. Martin, K. Morokuma, V. G. Zakrzewski, G. A. Voth, P. Salvador, J. J. Dannenberg, S. Dapprich, A. D. Daniels, O. Farkas, J. B. Foresman, J. V. Ortiz, J. Cioslowski and D. J. Fox, *Gaussian 09 Revis. C.01*, Gaussian, Inc., Wallingord, CT, 2010.
39 A. V. Marenich, C. J. Cramer and D. G. Truhlar, *J. Phys. Chem. B*, 2009, **113**, 6378–6396.
40 S. Plimpton, *J. Comput. Phys.*, 1995, **117**, 1–19.
41 W. D. Cornell, P. Cieplak, C. I. Bayly, I. R. Gould, K. M. Merz, D. M. Ferguson, D. C. Spellmeyer, T. Fox, J. W. Caldwell and P. A. Kollman, *J. Am. Chem. Soc.*, 1995, **117**, 5179–5197.
42 J. Wang, R. M. Wolf, J. W. Caldwell, P. A. Kollman and D. A. Case, *J. Comput. Chem.*, 2004, **25**, 1157–1174.
43 U. C. Singh and P. A. Kollman, *J. Comput. Chem.*, 1984, **5**, 129–145.
44 H. J. C. Berendsen, J. R. Grigera and T. P. Straatsma, *J. Phys. Chem.*, 1987, **91**, 6269–6271.
45 J. G. Harris and K. H. Yung, *J. Phys. Chem.*, 1995, **99**, 12021–12024.
46 S.-N. Huang, T. A. Pascal, W. A. Goddard, P. K. Maiti and S.-T. Lin, *J. Chem. Theory Comput.*, 2011, **7**, 1893–1901.
47 J.-P. Ryckaert, G. Ciccotti and H. J. C. Berendsen, *J. Comput. Phys.*, 1977, **23**, 327–341.
48 U. Essmann, L. Perera, M. L. Berkowitz, T. Darden, H. Lee and L. G. Pedersen, *J. Chem. Phys.*, 1995, **103**, 8577–8593.

49 W. G. Hoover, *Phys. Rev. A: At., Mol., Opt. Phys.*, 1985, **31**, 1695–1697.
50 S.-T. Lin, M. Blanco and W. A. Goddard, *J. Chem. Phys.*, 2003, **119**, 11792–11805.
51 S.-T. Lin, P. K. Maiti and W. A. Goddard, *J. Phys. Chem. B*, 2010, **114**, 8191–8198.
52 T. A. Pascal, S.-T. Lin and W. A. Goddard, *Phys. Chem. Chem. Phys.*, 2011, **13**, 169–181.
53 T. A. Pascal, D. Schärf, Y. Jung and T. D. Kühne, *J. Chem. Phys.*, 2012, **137**, 244507.
54 G. S. Hwang, H. M. Stowe, E. Paek and D. Manogaran, *Phys. Chem. Chem. Phys.*, 2015, **17**, 831–839.
55 H. M. Stowe, L. Vilčiauskas, E. Paek and G. S. Hwang, *Phys. Chem. Chem. Phys.*, 2015, **17**, 29184–29192.
56 S. A. Freeman and G. T. Rochelle, *J. Chem. Eng. Data*, 2011, **56**, 574–581.
57 C. Wang, X. Luo, X. Zhu, G. Cui, D. Jiang, D. Deng, H. Li and S. Dai, *RSC Adv.*, 2013, **3**, 15518–15527.
58 V. V. Chaban and N. A. Andreeva, *J. Chem. Eng. Data*, 2016, **61**, 1917–1923.
59 H. B. Hetzer, R. A. Robinson and R. G. Bates, *J. Phys. Chem.*, 1968, **72**, 2081–2086.
60 M. Brehm and B. Kirchner, *J. Chem. Inf. Model.*, 2011, **51**, 2007–2023.
61 X. Chen and G. T. Rochelle, *Chem. Eng. Res. Des.*, 2011, **89**, 1693–1710.
62 J. Liu, S. Wang, H. F. Svendsen, M. U. Idrees, I. Kim and C. Chen, *Int. J. Greenhouse Gas Control*, 2012, **9**, 148–159.
63 T. Lewis, M. Faubel, B. Winter and J. C. Hemminger, *Angew. Chem., Int. Ed.*, 2011, **50**, 10178–10181.
64 K. Robinson, A. McCluskey and M. I. Attalla, *ChemPhysChem*, 2011, **12**, 1088–1099.